THE JOURNAL OF PHYSICAL CHEMISTRY B

Article

pubs.acs.org/JPCB

Parallel β-Sheet Fibril and Antiparallel β-Sheet Oligomer: New Insights into Amyloid Formation of Hen Egg White Lysozyme under Heat and Acidic Condition from FTIR Spectroscopy

Ye Zou, Yiyi Li, Wenying Hao, Xiaoqian Hu, and Gang Ma*

Laboratory of Medicinal Chemistry and Molecular Diagnosis of Ministry of Education, College of Chemistry and Environmental Science, Hebei University, Baoding 071002, China

Supporting Information

ABSTRACT: Hen egg white lysozyme (HEWL) is widely used as a model protein for amyloid research. In this study, we aim to use Fourier transform infrared (FTIR) spectroscopy to gain new structural insights into amyloid formation of HEWL under heat and acidic condition. We reveal that the fibril-forming solution of HEWL has the capability to form fibril and oligomer with distinct β-sheet configurations under different temperatures. Amyloid fibril with parallel β-sheet configuration is formed at elevated temperature, while oligomer with antiparallel β-sheet configuration is formed at room temperature. The interplay between fibrillation and oligomerization suggests that the two β-sheet aggregates consume the same amyloidogenic materials such as peptide fragments and nicked HEWL due to lysozyme hydrolysis under heat and acidic condition. Temperature-dependent FTIR reveals that the oligomer is unstable at elevated temperature, demonstrating its off-pathway nature. The temperature-dependent formation of parallel and antiparallel β-sheet configurations discovered in lysozyme system is compared with that of amyloid-β and α-synuclein systems and the implication is discussed.

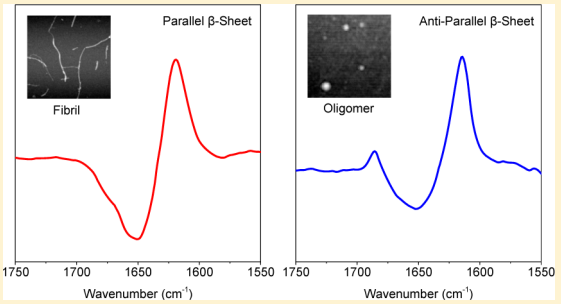

INTRODUCTION

Amyloid is a unique type of insoluble protein aggregate with a cross-β quaternary structure and fibrous morphology. The fibril architecture consists of extended and interdigitated β-sheets with the sheet running along the fibril axis and the strand running perpendicular to the fibril axis.[1] Such supramolecular configuration displays the characteristic ~4.8 and ~8−11 Å reflections in amyloid X-ray diffraction, which are attributed to the interstrand spacing and intersheet spacing, respectively.[1,2] When binding to the dye Congo red, amyloid fibrillar deposit displays apple green birefringence with polarizing optics.[3] In vivo, amyloid deposition is a pathological hallmark of more than 40 neurodegenerative, systemic, and nonsystemic diseases. These human amyloid diseases include some well-known disorders such as Alzheimer's disease, Parkinson's disease, and Type II diabetes. Each amyloid disease is associated with amyloid formation of one particular type of protein.[4] The apparent linkage between amyloid formation and amyloid disease makes designing and developing molecular intervention into amyloid formation a very promising strategy to prevent and treat amyloid diseases.[5]

Amyloid formation is a rather complex protein self-assembly process. It can follow nucleated polymerization mechanism where on-pathway oligomer is very hard to detect.[6] It can also follow nucleated conformational conversion mechanism where conformational conversion of on-pathway oligomeric precursor into fibril is observable.[6−9] Furthermore, there can be off-pathway oligomeric aggregates generated via nonfibril formation pathways.[10−13] The oligomeric aggregates in amyloid formation are in diverse size and morphology and have been referred to in numerous ways as amorphous aggregates, micelles, protofibrils, prefibrillar aggregates, globulomers, amylospheroids, and annular protofibrils.[14] Both mature fibril and nonfibrillar oligomer have been hypothesized to be the possible pathogenic agents in amyloid diseases and are thus important drug targets for developing molecular intervention into amyloid formation.[5] Given the therapeutic significance of the two aggregation species, structural characterization of fibril and oligomer is thus critically important and has indeed been a major research effort in the amyloid field.

It is now generally accepted that amyloid formation is a generic property pertaining to all proteins.[15,16] Numerous proteins not related to any amyloid disease have been discovered to form amyloid structure in vitro under appropriate conditions and have been used as model systems in amyloid study as well. Hen egg white lysozyme (HEWL) is one such representative example and it is widely used in amyloid research due to its well-characterized structure and its low cost.[17] Various methods have been used to induce amyloid formation of HEWL and all of them require destabilizing the native structure as a necessary step. These methods include heat and acidic condition,[18−23] heat and basic condition,[24] high

Received: January 11, 2013
Revised: February 26, 2013
Published: March 28, 2013

concentration of alcohol,[25] using sodium dodecyl sulfate as an inducer,[26] moderate concentration of guanidine hydrochloride,[27] heat with agitation,[28] and partial reduction with dithiolthreitol.[29] Among these methods, elevated temperature plus acidic condition is the most commonly chosen condition in studying fibrillation mechanism of HEWL and is being considered as the standard condition for fibrillation of HEWL.[19,22] The fibrils generated using such method display the most common amyloid fibril morphology, while some other methods usually generate amyloid-like structures.[24−27] The uniqueness of the heat and acidic method may lie in the fact that the combination of heat and acidic condition promotes HEWL hydrolysis, thus generating highly amyloidogenic peptide fragments.[19,22] The mature amyloid fibrils formed under heat and acidic condition were found mainly composed of fragments 49−101 and 53−101 as the core structure constituents instead of intact full-length HEWL.[22] The coexistence of hydrolysis and fibrillation makes HEWL amyloid formation even more complex than typical amyloid formation process.

Despite the extensive investigations on amyloid formation of HEWL under heat and acidic condition, information on the actual β-sheet configuration of HEWL fibril is still lacking. There are two types of β-sheet configurations, parallel or antiparallel. Such information is fundamentally important as this is the first issue that one would face when elucidating atomic or molecular structural details of amyloid fibrils.[1,30] Furthermore, recent study has demonstrated that parallel and antiparallel configurations could have distinct effects on the cytotoxicity of amyloid fibrils.[31] In this study, we will explore using Fourier transform infrared (FTIR) spectroscopy, in particular FTIR difference spectroscopy, to tackle this issue. Furthermore, we will perform a comparative study on an off-pathway β-sheet oligomer obtained by room-temperature incubation of fibril-forming solution by HEWL to gain deeper insight into the amyloid formation of HEWL. The interplay between fibrillation and oligomerization as well as the off-pathway nature of oligomer is also explored. The observed temperature-dependent formation of parallel and antiparallel β-sheet configurations in lysozyme system is compared with that of amyloid-β (Aβ) and α-synuclein systems and the implication is discussed.

EXPERIMENTAL AND METHODS

Materials. Hen egg white lysozyme (HEWL) (L6876) was obtained from Sigma-Aldrich (Saint Louis, MO) and used directly. Deuterium oxide (D_2O) with >99.8% purity was obtained from J&K Chemical (Beijing, China). Sodium chloride (NaCl) with >99% purity and deuterium chloride (DCl) (35% by weight in D_2O) were purchased from Sigma-Aldrich. Thioflavin T (ThT) was purchased from Acros (Geel, Belgium). Sodium azide (NaN_3) with a purity of 99% was purchased from Tianjin Chemical Plant (Tianjin, China). A short peptide segment of Aβ (Aβ_{8-28}) with purity of 98% by HPLC was purchased from ChinaPeptides (Shanghai, China). No further purification was performed on all the chemicals.

Solution Preparation and Incubation Conditions. HEWL solution in D_2O (pD = 2) containing 140 mM NaCl and 200 ppm NaN_3 was used for amyloid formation. Solution pH was adjusted using DCl solution in D_2O to reach a pH meter reading of 1.6 (pD = pH meter reading + 0.4).[32] The HEWL solution was first filtered with a 0.22 μm filter to remove possible large aggregates. HEWL concentration after filtration was determined by absorbance measurements using the extinction coefficient of 2.64 mL·mg^{-1}·cm^{-1} at 280 nm.[33] To obtain good signal-to-noise ratio in FTIR spectrum, a relatively high concentration (i.e., 15 mg/mL) of HEWL was used in this study. The HEWL solution in a sealed glass vial was incubated in a thermoshaker incubator at 62 °C without agitation. Aliquots of the fibril-forming solution were taken out of the incubation vial at different time points for characterization.

FTIR Spectroscopy. The FTIR spectra were obtained with a Bruker Vertex 70 FTIR spectrometer equipped with a DLaTGS detector. The sample compartment was constantly purged with dry air from a homemade purge system to further minimize water vapor interference. For measurements at room temperature of 25 °C, a demountable infrared (IR) cell with a pair of circular CaF_2 windows and a 50 μm spacer was used. For measurements at elevated temperatures, a sealed IR cell with a pair of circular CaF_2 windows and a 50 μm spacer was utilized. The edges of the IR cell were first glued together using the glue made by polystyrene and toluene and then the cell was dried in oven to solidify the glue. After sample injection, the sample inlets were also sealed with the glue and the glue will be dried during heating. The sealed IR cell can basically prevent solvent D_2O evaporation during FTIR measurements at elevated temperatures. A water bath with a temperature sensitivity of 0.1 °C and a water jacket were used to control the temperature of the cell. A digital temperature meter with a thermocouple was used for temperature reading. Spectra were collected with 4 cm^{-1} resolution and 128 scans. A factor of 4 was used for zero filling. With this level of zero filling, one wavenumber will correspond to one data point in the FTIR spectrum. FTIR data processing was performed with Bruker OPUS software. For difference spectroscopy, the subtraction factor may be slightly adjusted from the theoretical value of 1. This adjustment is to compensate some baseline drift and water absorption. The obtained difference spectrum was further corrected by subtracting a reference water vapor spectrum to remove water vapor interference using an approach similar to the protocol by Dong et al.[34] When making HEWL solutions, prior deuterium exchange on HEWL was not performed. When the HEWL in D_2O solution was incubated at 62 °C, the peptide backbone became fully deuterated during the lag phase as evidenced by the disappearance of the amide II band at 1540 cm^{-1} after 5 h incubation. Residual H_2O in the overwhelming D_2O forms HOD and has negligible effect on the spectral analysis in the amide I region. This approach eases the work of sample preparation and was used previously in a similar manner by others.[35] It should be pointed out that when we present FTIR spectra, solvent D_2O subtraction is not performed and the original spectra with only water vapor subtraction are directly presented.

Atomic Force Microscopy (AFM). All AFM images were taken on dried samples in air with Agilent Technologies 5500 scanning probe microscope in tapping mode. A 5 μm × 5 μm scanner was used throughout the AFM experiment. The silicon cantilevers were purchased from NT-MDT Instruments. The cantilever has a resonance frequency of 100 kHz and a nominal force constant of 3 N/m. The samples for AFM measurement were prepared using the following protocol: protein solution was diluted 300 times with deionized water from a Millipore system and then dropped onto freshly cleaved mica. After 20 min waiting time, the protein solution was rinsed off with deionized water. The mica surface was then dried with nitrogen

dx.doi.org/10.1021/jp4003559 | J. Phys. Chem. B 2013, 117, 4003−4013

flow and the sample was stored in a desiccator. AFM images were presented using the open-access software, Gwyddion.

ThT Fluorescence Assay. ThT fluorescence assay was performed with a Hitachi F-7000 fluorescence spectrophotometer. An excitation wavelength of 450 nm with a slit width of 5 nm and an emission wavelength of 486 nm with a slit width of 10 nm were used. The voltage of photomultiplier tube was set to 700 V. The concentration of ThT solution is 10 μM. The buffer is 20 mM phosphate buffer at pH = 7.4. The assay was performed ex situ. During fibrillation, aliquots of incubation solutions were taken out of the incubation vial at different time points and were subjected to the assay immediately. For each measurement, 10 μL of incubation solution was added into 1 mL of ThT solution in a 1.0 cm quartz cuvette. The solution in the cuvette was shaken first before each acquisition was run. Five acquisitions were averaged to give a final intensity reading at 486 nm. All measurements were performed in ambient conditions. Fitting of kinetic curve and determination of lag phase were performed according to the following empirical equation

$$Y = y_i + m_i x + \frac{y_f + m_f x}{1 + e^{-[(x-x_0)/\tau]}}$$

where Y is the ThT fluorescence intensity, x is the incubation time, and x_0 is the time to reach 50% of maximal ThT fluorescence; other parameters are determined by fitting. The lag time is defined by $x_0 - 2\tau$.[36]

RESULTS AND DISCUSSION

Fibrillation of HEWL. We first use ThT fluorescence assay and AFM to characterize the fibrillation process of HEWL. HEWL solution was incubated at pD=2 and 62 °C to induce fibril formation. At selected time points, aliquots of incubation solution were taken out of the incubation vial for ThT fluorescence measurements. We found that the fibrillation kinetics is affected by some uncontrollable parameters and the exact kinetic curve varies from sample to sample to some extent. Our observation is consistent with Arnaudov et al.'s observation in which they also found varied kinetics sample by sample with respect to the duration of lag phase and the growth rate when studying fibrillation of HEWL under heat and acidic condition.[20] This should be due to the fact that the kinetics of some amyloidogenic systems may be affected by stochastic nucleation to a greater extent, thus resulting in varied kinetics.[37−39] In Figure 1, we show one kinetic profile of HEWL fibrillation as a representative. It displays the typical sigmoidal shape with a lag phase, a growth phase, and an equilibrium phase. The curve was fitted according to the empirical function mentioned above and the lag phase was determined from three such kinetics measurements and found to be 46 ± 10 h. We also performed AFM measurements to confirm the presence of fibrils in the incubation solution, as ThT fluorescence enhancement at ∼485 nm is not specific to fibrillar structures. Shown in Figure 2A,B are the AFM images before and after fibrillation. At the lag phase, the mica surface is basically empty. At the equilibrium phase, we observed the formation of HEWL fibrillar aggregates with heights ranging from 3 to 4 nm.

One main purpose of this study is to determine the actual β-sheet configuration of HEWL fibril. This is in fact a long-standing unsolved issue in the amyloid formation of HEWL. We explore to use FTIR spectroscopy to tackle this issue.

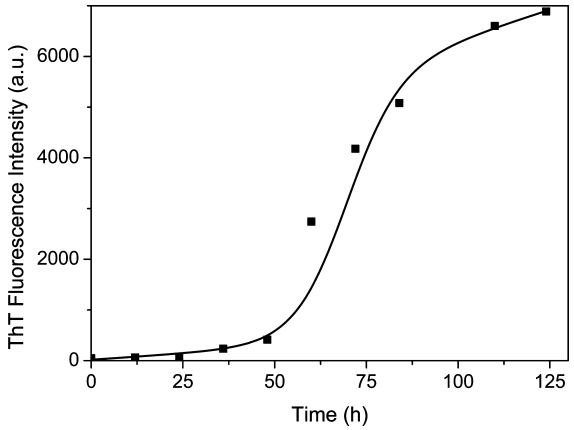

Figure 1. Fibrillation kinetics of HEWL under heat and acidic condition by ThT fluorescence assay: squares, experimental; line, fitting.

Vibrational spectroscopy, such as FTIR, has the capability to differentiate parallel and antiparallel β-sheet configurations in protein aggregates. This might be the most significant advantage of vibrational spectroscopy over circular dichroism (CD) spectroscopy. This capability lies in the fact that antiparallel β-sheet features with both a low-frequency component below 1640 cm^{-1} and a high-frequency component above 1680 cm^{-1} in the amide I (or amide I′) region; whereas parallel β-sheet structure lacks the high-frequency component above 1680 cm^{-1} and in fact displays a component between 1660 and 1670 cm^{-1}. Such assignment criterion was once questioned in the literature for the differentiation of β-sheet configurations in native proteins,[40] likely due to the fact that native protein structure is quite different from that of protein aggregates and lacks of large and extended β-sheet structure.[41,42] Yet, now increasing experimental and theoretical results support that this assignment criterion is applicable to differentiating antiparallel and parallel β-sheet structures in protein aggregates.[39,43−45] Evidence like these shows good correlations among experimental observations, theoretical simulations, and known structures. Ling et al. used theoretical calculation to demonstrate that the IR spectrum of a parallel β-sheet structure by 10 aligned β-strands displays one component at 1619 cm^{-1} and one high-frequency component at 1665 cm^{-1}.[44] Fu et al. used chiral-sensitive vibrational sum frequency generation spectroscopy to investigate human islet amyloid polypeptide (hIAPP) aggregates with known parallel β-sheet structure and revealed two vibrational bands at ∼1620 cm^{-1} and at ∼1660 cm^{-1}, respectively.[39] Sean used isotope-edited IR spectroscopy to demonstrate that a short amyloidogenic peptide forms in-register antiparallel β-sheet structure and this β-sheet structure features with one low-frequency component at ∼1620 cm^{-1} and one high-frequency component at ∼1686 cm^{-1}, respectively.[43] Very recently, Wang investigated both types of β-sheet configurations by several Aβ fragments including Aβ_{1-25}, Aβ_{25-35}, and Aβ_{33-42} using FTIR spectroscopy.[45] Their experimental and theoretical results further confirmed the validity of the above-mentioned peak-position criterion for parallel and antiparallel β-sheets assignments. Furthermore, there is also an empirical intensity-ratio criterion for antiparallel β-sheet assignment. That is the intensity ratio between the low-frequency component and the high-frequency component for an antiparallel β-sheet is about 8−10. Such an intensity-ratio criterion has been used to assign amyloid

dx.doi.org/10.1021/jp4003559 | J. Phys. Chem. B 2013, 117, 4003−4013

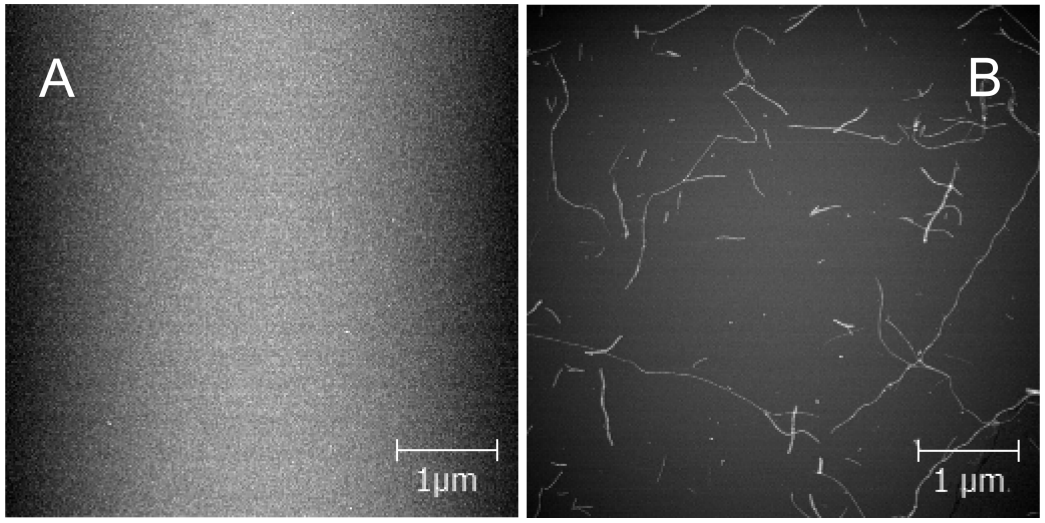

Figure 2. (A) AFM image for the aliquot from the incubation solution at 5 h time point in the lag phase. (B) AFM image for the aliquot from the incubation solution at 124 h time point in the equilibrium phase. Scale bar: 1 μm.

aggregates with antiparallel β-sheet configuration.[31,46,47] As in these studies about amyloid fibril structures,[31,47−50] we will use the above-mentioned criteria to perform IR assignments in the following investigation.

We aim to use FTIR difference spectroscopy to obtain the spectral features of HEWL fibrils. Ideally, when FTIR is used to monitor aggregation process, the incubation should be performed in the IR sample cell and the whole fibrillation process can then be monitored in situ by FTIR. Yet, it is extremely challenging to prevent solvent D_2O evaporation during the nearly week-long incubation at 62 °C for an only 50 μm thin layer of incubation solution sealed in the IR cell. We thus performed FTIR measurement in two alternative ways. To obtain spectra shown in Figure 3A, we took an aliquot of incubation solution out of the incubation vial at some point of the growth phase (i.e., at 72 h) and then injected it into the IR cell. The sealed IR cell was then kept at the incubation temperature of 62 °C, and the fibrillation process within the IR cell was monitored by in situ FTIR for five additional hours. Subtraction between FTIR spectra at a later time and an earlier time was then performed to give the difference spectrum. To obtain the spectra shown in Figure 3B, we performed ex situ FTIR measurements at 62 °C on two aliquots of the incubation solution obtained at two different time points (i.e., at 72h and 100 h) from the incubation vial. Subtraction between the two FTIR spectra gave the difference spectrum. The positive peaks in these difference spectra will reveal the component peaks that grow with fibrillation process. As revealed in Figure 3A,B, both of the different spectra show only one positive growth at 1618 cm^{-1} but lack a high-frequency component above 1680 cm^{-1}. Based on the above FTIR assignment criteria, this result suggests that HEWL fibril adopts a parallel β-sheet configuration. The 1660−1670 cm^{-1} band of the parallel β-sheet is buried within the broad negative peak of the difference spectrum, and thus not visible.

The above result from difference spectroscopy indeed suggests a parallel β-sheet configuration. Yet, to reach a final conclusion, one additional issue with respect to proper interpretation of the difference spectroscopy result has to be addressed. As we know, HEWL is a protein containing β-sheet structures, though the β-sheet content is very low. Previous studies reported that the β-sheet structure accounts for about

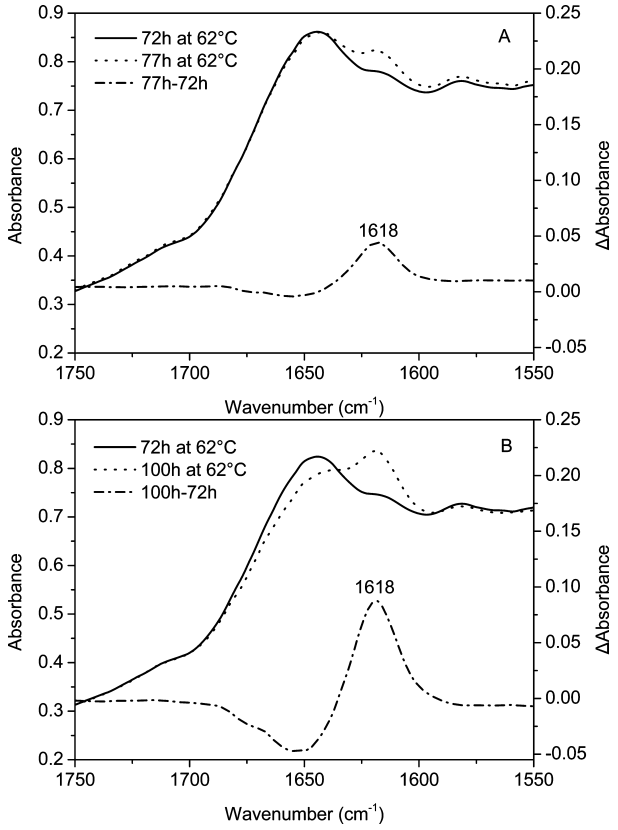

Figure 3. (A) FTIR spectra for the incubation solutions at 72 and 77 h measured at 62 °C and the difference spectrum between them. (B) FTIR spectra for the incubation solutions at 72 and 100 h time points measured at 62 °C and the difference spectrum between them. Left axis, original spectra; right axis, difference spectra; D_2O is not subtracted from original spectra.

6−7% of the total secondary structure.[51,52] We also used the online secondary structure assignment tool of Stride developed by Heinig and Frishman to analyze the crystal structure of HEWL (PDB ID: 193L, 1.33 Å resolution) and found in the total of 129 residues only eight are in β-sheet configurations, further confirming the low percentage of β-sheet content.[53]

dx.doi.org/10.1021/jp4003559 | J. Phys. Chem. B 2013, 117, 4003−4013

These β-sheets are antiparallel β-sheets and have some high-frequency IR absorption around 1685 cm^{-1} in amide I′ region.[51] This means that the following scenario could lead to a false conclusion from difference spectroscopy. If the total β-sheet content of the incubation solution after fibrillation is lower than that before fibrillation, even if the formed amyloid fibrils adopt antiparallel β-sheet configurations, it will be difficult to observe a positive peak above 1680 cm^{-1} in difference spectroscopy. This could lead us to falsely conclude that "since the high-frequency component is missing, the fibril should be in a parallel β-sheet configuration". Here, we argue that this will not be the case in the HEWL system because of the thermal unfolding of HEWL at 62 °C. Arnaudov et al. showed that the unfolding transition temperature of HEWL at pH = 2 is 55 °C and at around 60 °C HEWL becomes fully unfolded.[20] For unfolded HEWL, its native β-sheet structure will be destroyed and the native 1685 cm^{-1} absorbance will become negligible, thus not interfering with our difference spectroscopy interpretation. Since the above concern is removed, the only explanation of the observation in Figure 3 is that the HEWL fibrils are in parallel β-sheet configurations and thus do not have an absorbance above 1680 cm^{-1}. For a comparison, in a previous investigation about HEWL thermal aggregation in $D_2O-C_2H_5OD$ mixed solvent, the antiparallel β-sheet aggregates formed at 64 °C show an obvious absorbance increase at 1690 cm^{-1} along with an absorbance increase at 1618 cm^{-1}.[35]

Oligomerization of HEWL. Oligomerization and fibrillation are like the two sides of the same coin for amyloid formation. Low-temperature incubation is often used as a way to generate oligomeric aggregates as we see in the cases of Aβ and α-synuclein.[8,54,55] Theoretical prediction of the solubility diagram of fibrillogenic protein by Auser et al. also supports that oligomerization is not favored under elevated temperature.[9] In our previous investigation, we found that low-temperature (i.e., room temperature) incubation of the fibril-forming HEWL solution promotes oligomerization of HEWL.[56] We now perform a comparative structural investigation on oligomer and fibril and hope to gain deeper understanding of the complex aggregation behavior of HEWL under heat and acidic condition.

To induce oligomerization, at selected time points during fibrillation process, we took aliquots of the hot fibril-forming solution out of the incubation vial and performed further room-temperature incubation on these aliquots. The incubation can be done either directly in an IR cell or in an Eppendorf tube. Figure 4, A and B, shows the spectral variations during room-temperature incubation for aliquots at two selected time points of 28 and 56 h. For both of the samples, a prominent spectral growth between 1620 and 1600 cm^{-1} becomes observable during room-temperature incubation, suggesting the formation of some type of β-sheet aggregates. To further explore the nature of the spectral growth, we first obtained the more explicit feature of the spectra in Figure 4A,B using difference spectroscopy. The difference spectra were obtained by subtracting the spectrum at the beginning of the room-temperature incubation from that of a later time. Both of the difference spectra are also shown in Figure 4, and we further include a difference spectrum from the antiparallel β-sheet aggregates by Aβ_{8-28} peptide as assignment reference in Figure 4A. Two difference spectra of HEWL feature one low-frequency component at 1614 $cm^{-1}$and one high-frequency component at 1686 cm^{-1}, very similar to that of Aβ_{8-28}.

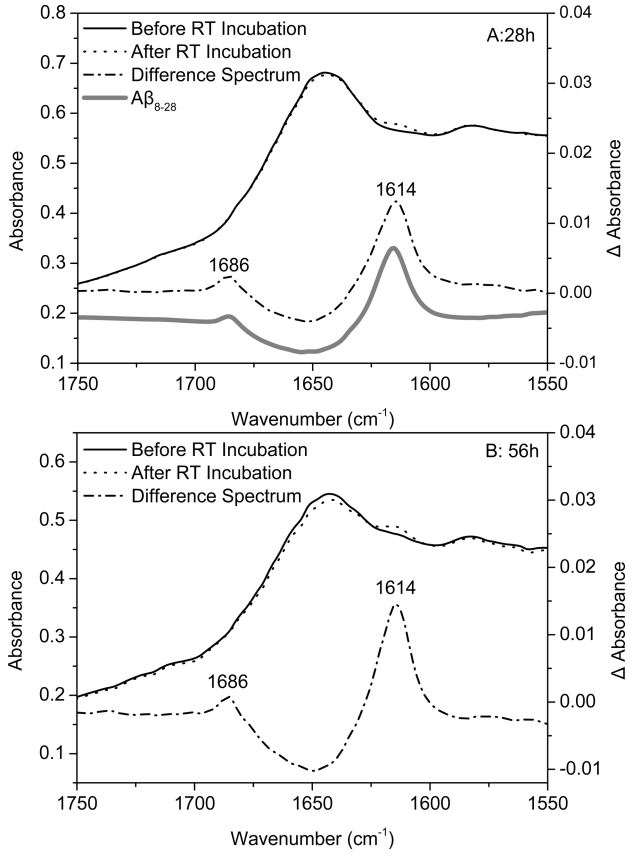

Figure 4. (A) Change in FTIR original spectra of the aliquot at 28 h time point before and after 20 min room-temperature incubation and the difference spectrum between them. (B) Change in FTIR original spectra of the aliquot at 56 h time point before and after 20 min room-temperature incubation and the difference spectrum between them. Left axis, original spectra; right axis, difference spectra; D_2O is not subtracted from original spectra. FTIR measurement was performed at room temperature (RT); an Aβ_{8-28} reference is also shown.

Furthermore, we measured the relative intensity ratio between 1614 cm^{-1} peak and 1686 cm^{-1} peak. The intensity of 1614 cm^{-1} peak is the integrated area between 1633.6 and 1600 cm^{-1}, while the intensity of 1686 cm^{-1} is the integrated area between 1700 and 1679 cm^{-1} and 1679 and 1633.6 cm^{-1} are positions of the two isoabsorptive points. The ratio for HEWL is found to be ~9, similar to the ratio for Aβ_{8-28}, which is ~10. According to the assignment criteria for antiparallel β-sheet structure discussed above, these spectral parameters suggest that the β-sheet aggregates of HEWL formed under room-temperature incubation are in antiparallel β-sheet configurations.

Here, before ending the assignment session, we would like to address one complication in antiparallel β-sheet assignment. It is now well-known that amyloid fibrils or oligomers often contain turn structure. This is particularly true if the fibrils or oligomers are formed by relatively long peptide strands such as Aβ_{1-42}, Aβ_{1-40}, and hIAPP.[8,57−59] The amide I frequency of turn can overlap with the high-frequency mode of antiparallel β-sheet, thus complicating spectral assignment.[60] For example, Strasfeld et al. investigated the amyloid fibril structure of hIAPP using two-dimensional infrared (2D-IR) spectroscopy and the turn structure was observed at 1685 cm^{-1} in the amide I′ region.[61] This spectral assignment is based on the empirical value of turn and spectral simulation, and is in agreement with

dx.doi.org/10.1021/jp4003559 | J. Phys. Chem. B 2013, 117, 4003−4013

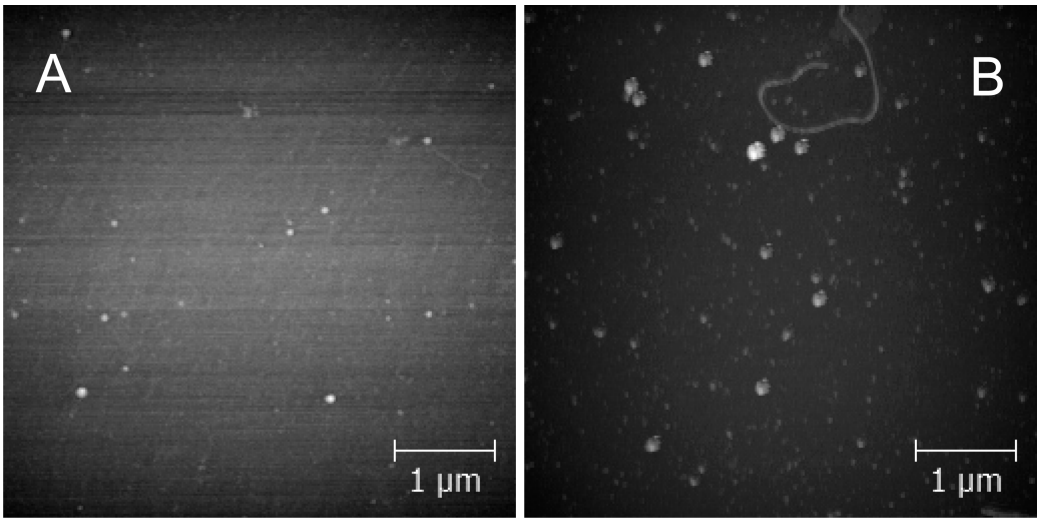

Figure 5. (A) AFM image of the aliquot at 28 h time point after 20 min room-temperature incubation. (B) AFM image of the aliquot at 56 h time point after 20 min room-temperature incubation. Scale bar: 1 μm.

the observed polarization dependence of the cross peaks and the isotope effect in 2D-IR spectroscopy. Therefore, one may argue that whether the observed 1686 cm^{-1} in our study could be from turn. Indeed, the amyloidogenic HEWL peptide fragments of 49−101 and 53−101 are approximately 50-residue long which is about 20-residue longer than the 8−37 fragment of hIAPP. Such a long strand should form turn structures in β-sheet aggregates such as amyloid fibrils or oligomers. However, as shown in Figure 3, when HEWL forms parallel β-sheet fibrils, we did not observe any peak corresponding to turn structure in the difference spectrum above 1680 cm^{-1}. This suggests that the IR signature of turn structure formed by the HEWL peptide fragments is below 1680 cm^{-1}. This is possible as previously observed amide I frequencies of turn structures vary in a relatively large range. It can be from 1653 to 1691 cm^{-1} in the amide I′ region.[40] Therefore, the spectral comparison between Figures 3 and 4 in fact provides an additional evidence to support our 1686 cm^{-1} peak assignment.

We further performed AFM study to reveal the morphological nature of these aggregates formed under room temperature. Figure 5, A and B, shows the AFM images corresponding to the 28 and 56 h aliquots in Figure 4. Both of the images reveal the presence of oligomeric aggregates with heights ranging from 2 to 8 nm. And the more conclusive information about the oligomer nature of the 1614 cm^{-1} comes from Figure 5A. The 28 h time point is in the lag phase and there is no fibril present in the incubation solution. In Figure 5A, all we see are oligomeric aggregates and no fibril can be observed. This means that the antiparallel β-sheet aggregates formed at room-temperature are oligomers rather than fibrils. Here, one may wonder whether prolonged incubation under room temperature can result in oligomer-to-fibril conversion since some amyloidogenic systems can take weeks or even months to finally transform into fibrils. We did not explore such long-term incubation. What we assert is that the observed spectral growths at 1614 cm^{-1} and 1686 cm^{-1} in the FTIR spectra in Figure 4 correspond to the observed oligomeric aggregates in AFM within our observation time window. According to Auser et al.'s theoretical model of fibril nucleation, fibrillation pathway can follow one-step or two-step nucleation.[9] In two-step nucleation, there are situations that the oligomers are not kinetically competent to convert into fibrils and the solution is thus populated solely by oligomers. The oligomerization situation in our study may belong to this case within our observation time window.

The room-temperature oligomerization of HEWL presented above has two important implications. First, the oligomerization study reveals a very interesting feature of the fibril-forming HEWL incubation solution. That is, the incubation solution has the capability to form two distinct β-sheet aggregates, parallel β-sheet fibrils, and antiparallel β-sheet oligomers, under two different incubation temperatures (elevated temperature and room temperature). Second, the difference spectrum of oligomer in fact serves as additional supportive evidence for the parallel β-sheet structure of HEWL fibril. Figure 6 shows

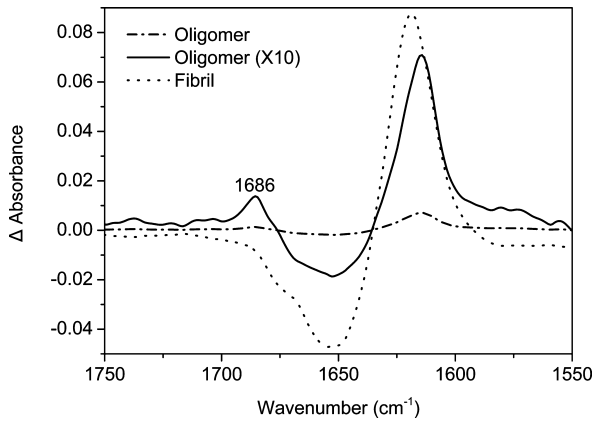

Figure 6. Spectral comparison between fibril and oligomer.

the spectral comparison between the difference spectra corresponding to fibril and oligomer. The difference spectrum of oligomer is obtained with very short incubation time at room temperature, thus having a very small absorbance at 1614 cm^{-1}. The absorbance of 1614 cm^{-1} oligomer peak is only 1/12 of that of the 1618 cm^{-1} fibril peak. Yet, in the oligomer difference spectrum, the high-frequency 1686 cm^{-1} peak is still quite obvious above the noisy baseline as clearly revealed in the 10× magnified oligomer spectrum. This implies that, if HEWL fibril adopted an antiparallel β-sheet configuration, its difference spectrum should have been able to reveal a high-frequency peak

dx.doi.org/10.1021/jp4003559 | J. Phys. Chem. B 2013, 117, 4003−4013

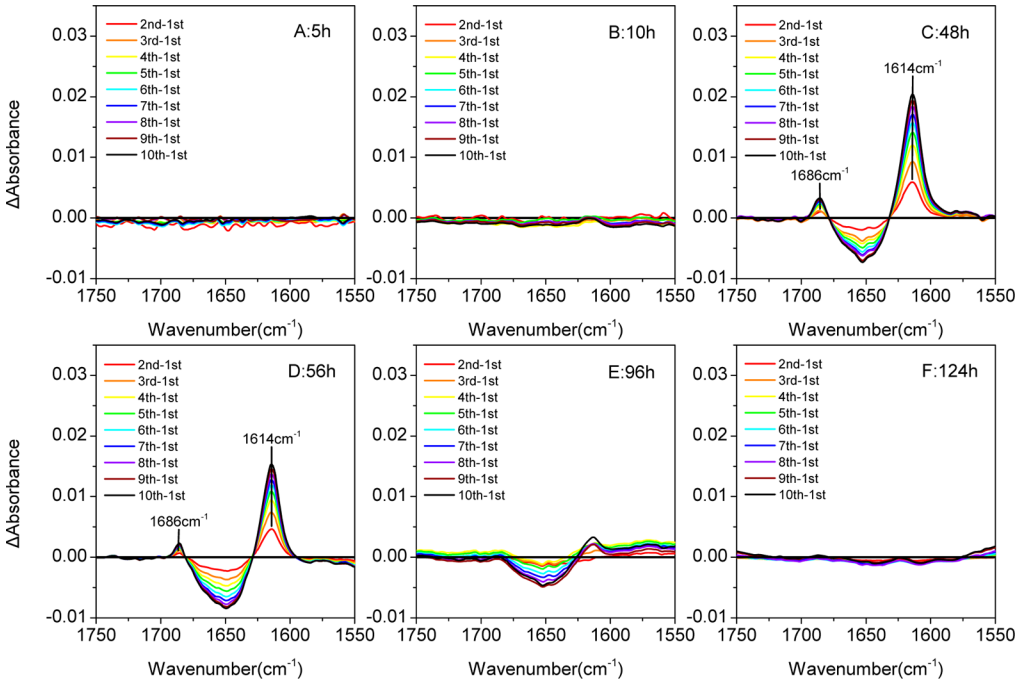

Figure 7. Room-temperature oligomerization capabilities of the aliquots taken at different time points characterized by difference spectroscopy. A–F: difference spectra obtained from the spectral sets for 5, 10, 48, 56, 96, and 124 h aliquots. The first spectrum of each spectral set (first) is used as subtraction reference.

above 1680 cm^{-1}. Therefore, the missing of the high-frequency component in the difference spectrum of fibril is a "true" missing due to the parallel β-sheet configuration and not due to detection sensitivity issue.

Interplay between Fibrillation and Oligomerization. Heat and acidic condition promote hydrolysis of HEWL at 48 and 101 Asp residue sites and generate highly amyloidogenic peptide fragments of 49–101 and 53–101 as well as nicked HEWL with these fragments.[22] These fragments are the amyloidogenic materials responsible for the fibrillation of HEWL under heat and acidic condition. The matrix-assisted laser desorption/ionization time-of-flight (MALDI-TOF) result indicated that fibril mainly constitutes the amyloidogenic fragments of 48–101 and 53–101, while the 19–119 fragment and nicked full-length HEWL are minor components. The counterpart fragment of 1–48/102–129 is nonamyloidogenic.[22]

The composition complexity of the HEWL incubation solution raises an issue with respect to the relationship between fibrillation and oligomerization. That is whether fibrillation and oligomerization consume the same amyloidogenic materials (fragments and nicked HEWL). We should not exclude the possibility that fibrils and oligomers are composed of different peptide fragments. To tackle this issue, we studied the oligomerization capability of fibril-forming HEWL incubation solution at different time points during fibrillation. We took aliquots of the hot HEWL solution out of the incubation vial at different time points and performed room-temperature incubation on these aliquots within the IR cell. These aliquots were monitored in situ for the same period of time (i.e., 20 min). For each aliquot, a set of 10 spectra were taken. We then evaluated the extent of oligomerization of the fibril-forming solution by following the growth of the oligomer component peak at 1614 and 1686 cm^{-1} over time using difference spectroscopy. When performing difference spectroscopy, we took the first spectrum in each spectral set as subtraction reference to generate nine difference spectra. Shown in Figure 7, at the beginning of the lag phase (i.e., 5 h in Figure 7A and 10 h in Figure 7B), no spectral growth is observed, indicating the absence of oligomerization. At the late lag phase and in the growth phase (i.e., 48 h in Figure 7C and 56 h in Figure 7D), prominent spectral growths can be observed at 1614 and 1686 cm^{-1}, similar to the observation in Figure 4. The relative intensity ratios between 1614 and 1686 cm^{-1} components as listed in Table S1 in the Supporting Information are also found similar to that in Figure 4, thus confirming the oligomerization nature of such spectral growths; at the equilibrium phase (i.e., 96 h in Figure 7E and 124 h in Figure 7F), no obvious spectral growth is observed, indicating negligible oligomerization. Clearly, the capability of the fibril-forming incubation solution to form oligomer depends on the extent of fibrillation. The observed phenomenon in Figure 7 can be easily explained by assuming that fibrillation and oligomerization are consuming the same amyloidogenic materials. At 5 and 10 h, due to the low concentration of amyloidogenic fragments generated by hydrolysis, oligomerization is negligible as indicated by the absence of any spectral growth over time. At 48 and 56 h, there are a large amount of amyloidogenic fragments in the incubation solution. This results in a prominent oligomerization upon room-temperature incubation as indicated by the obvious spectral growths at 1614 and 1686 cm^{-1} over time. Once the incubation solution enters into the fibrillation equilibrium phase, since most of the amyloidogenic materials have been converted into fibril and almost no materials can be recruited by oligomerization, oligomerization process thus becomes negligible again. This is why we observe the basically negligible spectral growth at 96 and 124 h which are in the fibrillation equilibrium phase. Therefore, the above analysis with respect to the interplay between fibrillation and oligomerization supports that HEWL fibrils and oligomers are composed of the same

dx.doi.org/10.1021/jp4003559 | J. Phys. Chem. B 2013, 117, 4003–4013

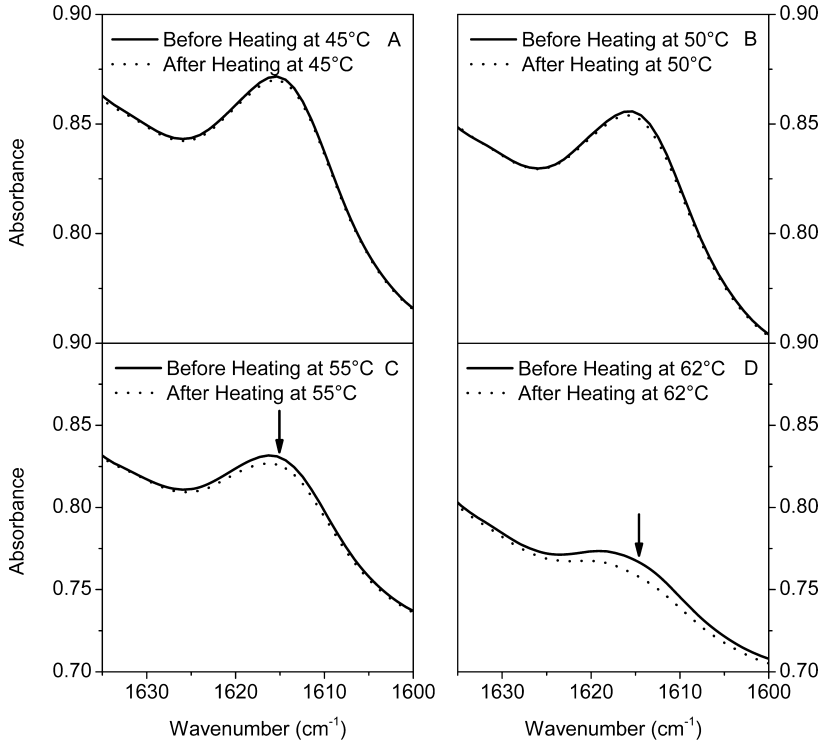

Figure 8. Thermal stability of oligomer characterized by FTIR spectral variation around 1614 cm^{-1}. A–D: 45, 50, 55, and 62 °C. D_2O is not subtracted from original spectra.

amyloidogenic materials, probably mainly the fragments of 48–101 and 53–101.

Previous investigation about the aggregation propensities of HEWL peptide fragments by Frare et al. using the prediction method by Dubay et al. showed that the propensity index of 50–101 is 0.34, while that of 1–47/102–129 is −3.3.[19] The much lower negative value of 1–47/102–129 is an indicator of its low aggregation propensity.[62] CD studies by Frare et al. also reveal that 57–101 is the highly amyloidogenic fragment responsible for HEWL fibrillation, while 1–32/102–129 remained largely disordered in solution and does not show fibrillation even for prolonged incubation.[19] This evidence again supports that formations of fibril and oligomer should be due to the aggregation of 48–101 and 53–101 fragments (and nicked HEWL with these fragments).

Thermal Stability of Oligomer under Elevated Temperature and Its off-Pathway Nature. Since the oligomer is obtained by incubating the fibril-forming solution of HEWL at room temperature, one may be curious about the fate of oligomer at elevated temperatures. To explore this issue, we first incubated the fibril-forming solution for some period of time to generate some amount of oligomer (characteristic with the growth of 1614 cm^{-1} component in FTIR spectrum). Then we subjected the oligomer-containing solution to different temperatures to test its thermal stability by monitoring the decease of the characteristic 1614 cm^{-1} component peak. A decreased 1614 cm^{-1} component upon heating is an indicator to the thermal instability of oligomer. Figure 8 shows the results for oligomer subjected to temperature ramp in an IR cell. The oligomers were formed by room-temperature incubation of a 48 h time point aliquot. At each temperature, the sample was equilibrated for 10 min first and then heated for another 30 min. As shown in Figure 8, the oligomers are stable at 45 and 50 °C, but unstable at 55 and 62 °C. We should point out that, in our previous study, we once stated that these oligomeric aggregates can still be present at 62 °C.[56] We now realize that this statement is not accurate as once decomposition happens, a full decomposition will be just a matter of time. To further illustrate this point, we studied the dissociation of the 1614 cm^{-1} oligomer at 62 °C alone. In Figure 9, "A" is the original spectrum taken at 62 °C of an aliquot without oligomer, "B" is the spectrum taken at room temperature after some oligomer formation through room-temperature incubation, and "C" is the spectrum taken at 62 °C after oligomer dissociation. The overlap between A and C demonstrates the fully dissociation of oligomer due to heating at 62 °C. In fact, the formation and

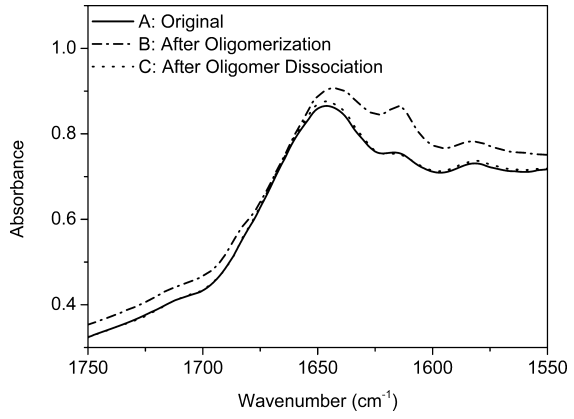

Figure 9. Thermal dissociation of oligomer at 62 °C characterized by FTIR spectral variation around 1614 cm^{-1}. A, original spectrum at 62 °C; B, after oligomer formation at room temperature; C, after oligomer dissociation at 62 °C. Baseline shift in B is due to the temperature effect on the spectrum of solvent D_2O. D_2O is not subtracted from original spectra.

dx.doi.org/10.1021/jp4003559 | J. Phys. Chem. B 2013, 117, 4003–4013

dissociation of oligomer shown in Figure 9 can be cycled in situ within the IR cell by thermal cycles (data not shown).

The thermal stability study here has one important implication. That is, it reveals the off-pathway nature of the 1614 cm^{-1} oligomer. Since oligomer is unstable and decomposes at the incubation temperature of 62 °C, it is thus impossible for this oligomer to be present as an on-pathway intermediate. Therefore, if we want to transform the antiparallel β-sheet oligomer into parallel β-sheet fibril, we would have to dissociate the antiparallel β-sheer oligomer in the first place. This situation reminds us of a similar observation in a very recent report about the fibrillation behavior of an Aβ mutant, D23N-Aβ_{1-40}. Qiang et al. found that D23N-Aβ_{1-40} has the capability to form both parallel β-sheet fibril and antiparallel β-sheet fibril.[63] However, the antiparallel β-sheet fibril is thermodynamically metastable and can transform into parallel β-sheet fibril by gradual dissolution of the antiparallel β-sheet fibril.

Comparison with Aβ and α-Synuclein and Its Implication. Our study reveals that the fibril-forming HEWL solution (i.e., the amyloidogenic HEWL peptide fragments) has the capability to form fibril and oligomer with distinct β-sheet configurations under different temperatures. Fibrils adopt parallel β-sheet configurations at high temperature while oligomers adopt antiparallel β-sheet configurations at low temperature. This interesting observation inspires us to compare the HEWL system with the other two amyloid systems that were also shown to possess such capability. The two amyloid systems are the well-known Aβ and α-synuclein. The former is relevant to Alzheimer's disease and the latter to Parkinson's disease. In one recent study, Cerf et al. used FTIR spectroscopy to investigate the β-sheet configurations of oligomer and fibril by Aβ.[55] The oligomer formed with 4 °C incubation displays characteristic antiparallel β-sheet IR frequencies at ~1630 and ~1695 cm^{-1}, while the fibril formed with 37 °C incubation displays characteristic parallel β-sheet frequencies at ~1630 and ~1665 cm^{-1}. Similar observation can be found in another recent report on α-synuclein by Celej et al. where the oligomer formed with 25 °C incubation displays characteristic antiparallel β-sheet IR frequencies at 1625 and 1695 cm^{-1}, while the fibril formed with 37 or 70 °C incubation displays parallel β-sheet frequencies at 1628 and ~1665 cm^{-1}.[49] The temperature-dependent formation of parallel and antiparallel β-sheet configurations was in fact not pointed out in these studies about Aβ and α-synuclein, yet the results in these studies clearly demonstrated this point. With this respect, HEWL system in our study is similar to Aβ and α-synuclein with respect to the fact that they all possess the capabilities to adopt distinct β-sheet configurations under different temperatures. However, they are different in other aspects. HEWL oligomer in our study is of off-pathway nature as revealed by thermal stability study, while oligomers of Aβ and α-synuclein were assumed to be of on-pathway nature supported by AFM or seeding experiment.[48,49] The on-pathway nature requires the β-sheet in these oligomers to be intramolecular β-sheet,[48] while the β-sheet in HEWL oligomer is intermolecular.

To our knowledge, besides Aβ and α-synuclein, the amyloidogenic HEWL peptide fragments in our study might be the third amyloid system that was found to be able to form parallel β-sheet fibril and antiparallel β-sheet oligomer under different temperatures. Can other amyloidogenic peptides be found to have such capability? How does temperature play its role in determining the actual β-sheet configuration? These are open questions yet to be answered in the future.

CONCLUSIONS

Amyloid formation of HEWL under heat and acidic condition was investigated by FTIR spectroscopy along with AFM and ThT fluorescence and new structural insights with respect to fibrillation and oligomerization were obtained. With FTIR difference spectroscopy, we revealed that the fibril formed under elevated temperature adopts a parallel β-sheet configuration while the oligomer formed under room temperature adopts an antiparallel β-sheet configuration. The interplay between these two processes demonstrates that the two β-sheet aggregates are composed of the same amyloidogenic materials in the fibril-forming HEWL solution. Temperature-dependent FTIR study supports the off-pathway nature of oligomer. The observed property of temperature-dependent formation of distinct β-sheet configurations in this study is compared with that in Aβ and α-synuclein systems.

ASSOCIATED CONTENT

Supporting Information

Table S1 containing information about the relative intensity ratios between the 1614 cm^{-1} peak and 1686 cm^{-1} peak in Figure 7, C and D. This material is available free of charge via the Internet at http://pubs.acs.org.

AUTHOR INFORMATION

Corresponding Author

*E-mail: gangma@hbu.edu.cn.

Notes

The authors declare no competing financial interest.

ACKNOWLEDGMENTS

We gratefully acknowledge the financial support from the National Natural Science Foundation of China (No. 21075027), the Natural Science Foundation of Hebei Province (No. B2011201082), the Key Project of Chinese Ministry of Education (No. 211014), JUREN Plan of Hebei Province, and Hebei University startup fund (2010-184).

ABBREVIATIONS

HEWL, hen egg white lysozyme; Aβ, amyloid-β; hIAPP, human islet amyloid polypeptide; D_2O, deuterium oxide; NaCl, sodium chloride; DCl, deuterium chloride; ThT, thioflavin T; NaN_3, sodium azide; FTIR, Fourier transform infrared; IR, infrared; 2D-IR, two-dimensional Infrared; AFM, atomic force microscopy; CD, circular dichroism; MALDI-TOF, matrix-assisted laser desorption/ionization time of flight

REFERENCES

(1) Sawaya, M. R.; Sambashivan, S.; Nelson, R.; Ivanova, M. I.; Sievers, S. A.; Apostol, M. I.; Thompson, M. J.; Balbirnie, M.; Wiltzius, J. J. W.; McFarlane, H. T.; et al. Atomic Structures of Amyloid Cross-Beta Spines Reveal Varied Steric Zippers. *Nature* **2007**, *447*, 453−457.

(2) Margittai, M.; Langen, R. Fibrils with Parallel in-Register Structure Constitute a Major Class of Amyloid Fibrils: Molecular Insights from Electron Paramagnetic Resonance Spectroscopy. *Q. Rev. Biophys.* **2008**, *41*, 265−297.

(3) Sipe, J. D.; Cohen, A. S. Review: History of the Amyloid Fibril. *J. Struct. Biol.* **2000**, *130*, 88−98.

(4) Chiti, F.; Dobson, C. M. Protein Misfolding, Functional Amyloid, and Human Disease. *Annu. Rev. Biochem.* **2006**, *75*, 333−366.

(5) Lansbury, P. T.; Lashuel, H. A. A Century-Old Debate on Protein Aggregation and Neurodegeneration Enters the Clinic. *Nature* **2006**, *443*, 774−779.
(6) Lee, J.; Culyba, E. K.; Powers, E. T.; Kelly, J. W. Amyloid-Beta Forms Fibrils by Nucleated Conformational Conversion of Oligomers. *Nat. Chem. Biol.* **2011**, *7*, 602−609.
(7) Serio, T. R.; Cashikar, A. G.; Kowal, A. S.; Sawicki, G. J.; Moslehi, J. J.; Serpell, L.; Arnsdorf, M. F.; Lindquist, S. L. Nucleated Conformational Conversion and the Replication of Conformational Information by a Prion Determinant. *Science* **2000**, *289*, 1317−1321.
(8) Ahmed, M.; Davis, J.; Aucoin, D.; Sato, T.; Ahuja, S.; Aimoto, S.; Elliott, J. I.; Van Nostrand, W. E.; Smith, S. O. Structural Conversion of Neurotoxic Amyloid-Beta(1−42) Oligomers to Fibrils. *Nat. Struct. Mol. Biol.* **2010**, *17*, 561−567.
(9) Auer, S.; Ricchiuto, P.; Kashchiev, D. Two-Step Nucleation of Amyloid Fibrils: Omnipresent or Not? *J. Mol. Biol.* **2012**, *422*, 723−730.
(10) Gellermann, G. P.; Byrnes, H.; Striebinger, A.; Ullrich, K.; Mueller, R.; Hillen, H.; Barghorn, S. Abeta-Globulomers are Formed Independently of the Fibril Pathway. *Neurobiol. Dis.* **2008**, *30*, 212−220.
(11) Kayed, R.; Pensalfini, A.; Margol, L.; Sokolov, Y.; Sarsoza, F.; Head, E.; Hall, J.; Glabe, C. Annular Protofibrils are a Structurally and Functionally Distinct Type of Amyloid Oligomer. *J. Biol. Chem.* **2009**, *284*, 4230−4237.
(12) Kumar, A.; Paslay, L. C.; Lyons, D.; Morgan, S. E.; Correia, J. J.; Rangachari, V. Specific Soluble Oligomers of Amyloid-Beta Peptide Undergo Replication and Form Non-Fibrillar Aggregates in Interfacial Environments. *J. Biol. Chem.* **2012**, *287*, 21253−21264.
(13) Laganowsky, A.; Liu, C.; Sawaya, M. R.; Whitelegge, J. P.; Park, J.; Zhao, M.; Pensalfini, A.; Soriaga, A. B.; Landau, M.; Teng, P. K.; et al. Atomic View of a Toxic Amyloid Small Oligomer. *Science* **2012**, *335*, 1228−1231.
(14) Glabe, C. G. Structural Classification of Toxic Amyloid Oligomers. *J. Biol. Chem.* **2008**, *283*, 29639−19643.
(15) Chiti, F.; Webster, P.; Taddei, N.; Clark, A.; Stefani, M.; Ramponi, G.; Dobson, C. M. Designing Conditions for in Vitro Formation of Amyloid Protofilaments and Fibrils. *Proc. Natl. Acad. Sci. U.S.A.* **1999**, *96*, 3590−3594.
(16) Dobson, C. M. Protein Folding and Misfolding. *Nature* **2003**, *426*, 884−890.
(17) Trexler, A. J.; Nilsson, M. R. The Formation of Amyloid Fibrils from Proteins in the Lysozyme Family. *Curr. Protein Pept. Sci.* **2007**, *8*, 537−557.
(18) Krebs, M. R. H.; Wilkins, D. K.; Chung, E. W.; Pitkeathly, M. C.; Chamberlain, A. K.; Zurdo, J.; Robinson, C. V.; Dobson, C. M. Formation and Seeding of Amyloid Fibrils from Wild-Type Hen Lysozyme and a Peptide Fragment from the Beta-Domain. *J. Mol. Biol.* **2000**, *300*, 541−549.
(19) Frare, E.; P.; P., D. L.; Zurdo, J.; Dobson, C. M.; Fontana, A. A Highly Amyloidogenic Region of Hen Lysozyme. *J. Mol. Biol.* **2004**, *340*, 1153−1165.
(20) Arnaudov, L. N.; de Vries, R. Thermally Induced Fibrillar Aggregation of Hen Egg White Lysozyme. *Biophys. J.* **2005**, *88*, 515−526.
(21) Shashilov, V.; Xu, M.; Ermolenkov, V. V.; Fredriksen, L.; Lednev, I. K. Probing a Fibrillation Nucleus Directly by Deep Ultraviolet Raman Spectroscopy. *J. Am. Chem. Soc.* **2007**, *129*, 6972−6973.
(22) Mishra, R.; Sorgjerd, K.; Nystrom, S.; Nordigarden, A.; Yu, Y.-C.; Hammarstrom, P. Lysozyme Amyloidogenesis is Accelerated by Specific Nicking and Fragmentation but Decelerated by Intact Protein Binding and Conversion. *J. Mol. Biol.* **2007**, *366*, 1029−1044.
(23) Hill, S. E.; Robinson, J.; Matthews, G.; Muschol, M. Amyloid Protofibrils of Lysozyme Nucleate and Grow Via Oligomer Fusion. *Biophys. J.* **2009**, *96*, 3781−3790.
(24) Kumar, S.; Ravi, V. K.; Swaminathan, R. How Do Surfactants and DTT Affect the Size, Dynamics, Activity and Growth of Soluble Lysozyme Aggregates? *Biochem. J.* **2008**, *415*, 275−288.
(25) Goda, S.; Takano, K.; Yamagata, Y.; Nagata, R.; Akutsu, H.; Maki, S.; Namba, K.; Yutani, K. Amyloid Protofilament Formation of Hen Egg Lysozyme in Highly Concentrated Ethanol Solution. *Protein Sci.* **2000**, *9*, 369−375.
(26) Khan, J. M.; Qadeer, A.; Chaturvedi, S. K.; Ahmad, E.; Rehman, S. A.; Gourinath, S.; Khan, R. H. SDS Can Be Utilized as an Amyloid Inducer: A Case Study on Diverse Proteins. *PLoS One* **2012**, *7*, e29694.
(27) Vernaglia, B. A.; Huang, J.; Clark, E. D. Guanidine Hydrochloride Can Induce Amyloid Fibril Formation from Hen Egg-White Lysozyme. *Biomacromolecules* **2004**, *5*, 1362−1370.
(28) Sasahara, K.; Yagi, H.; Naiki, H.; Goto, Y. Heat-Induced Conversion of Beta(2)-Microglobulin and Hen Egg-White Lysozyme into Amyloid Fibrils. *J. Mol. Biol.* **2007**, *372*, 981−991.
(29) Takase, K.; Higashi, T.; Omura, T. Aggregate Formation and the Structure of the Aggregates of Disulfide-Reduced Proteins. *J. Protein Chem.* **2002**, *21*, 427−433.
(30) Stroud, J. C.; Liu, C.; Teng, P. K.; Eisenberg, D. Toxic Fibrillar Oligomers of Amyloid-Beta Have Cross-Beta Structure. *Proc. Natl. Acad. Sci. U.S.A.* **2012**, *109*, 7717−7722.
(31) Berthelot, K.; Ta, H. P.; Gean, J.; Lecomte, S.; Cullin, C. In Vivo and in Vitro Analyses of Toxic Mutants of HET-s: FTIR Antiparallel Signature Correlates with Amyloid Toxicity. *J. Mol. Biol.* **2011**, *412*, 137−152.
(32) Lumry, R.; Smith, E. L.; Glantz, R. R. Kinetics of Carboxypeptidase Action. I. Effect of Various Extrinsic Factors on Kinetic Parameters. *J. Am. Chem. Soc.* **1951**, *73*, 4330−4340.
(33) Aune, K. C.; Tanford, C. Thermodynamics of the Denaturation of Lysozyme by Guanidine Hydrochloride. I. Depdendence on pH at 25 Degrees. *Biochemistry* **1969**, *8*, 4579−4585.
(34) Dong, A.; Caughey, W. S. Infrared Methods for Study of Hemoglobin Reactions and Structures. *Methods Enzymol.* **1994**, *232*, 139−175.
(35) Sassi, P.; Giugliarelli, A.; Paolantoni, M.; Morresi, A.; Onori, G. Unfolding and Aggregation of Lysozyme: A Thermodynamic and Kinetic Study by FTIR Spectroscopy. *Biophys. Chem.* **2011**, *158*, 46−53.
(36) Nielsen, L.; Khurana, R.; Coats, A.; Frokjaer, S.; Brange, J.; Vyas, S.; Uversky, V. N.; Fink, A. L. Effect of Environmental Factors on the Kinetics of Insulin Fibril Formation: Elucidation of the Molecular Mechanism. *Biochemistry* **2001**, *40*, 6036−6046.
(37) Harper, J. D.; Lansbury, P. T. J. Models of Amyloid Seeding in Alzheimer's Disease and Scrapie:Mechanistic Truths and Physiological Consequences of the Time-Dependent Solubility of Amyloid Proteins. *Annu. Rev. Biochem.* **1997**, *66*, 385−407.
(38) Hortschansky, P.; Schroeckh, V.; Christopeit, T.; Zandomeneghi, G.; Fändrich, M. The Aggregation Kinetics of Alzheimer's Beta-Amyloid Peptide is Controlled by Stochastic Nucleation. *Protein Sci.* **2005**, *14*, 1753−1759.
(39) Fu, L.; Ma, G.; Yan, E. C. Y. In Situ Misfolding of Human Islet Amyloid Polypeptide at Interfaces Probed by Vibrational Sum Frequency Generation. *J. Am. Chem. Soc.* **2010**, *132*, 5405−5412.
(40) Barth, A.; Zscherp, C. What Vibrations Tell Us About Proteins. *Q. Rev. Biophys.* **2002**, *35*, 369−430.
(41) Kubelka, J.; Keiderling, T. A. Differentiation of Beta-Sheet-Forming Structures: Ab Initio-Based Simulations of IR Absorption and Vibrational CD for Model Peptide and Protein Beta-Sheets. *J. Am. Chem. Soc.* **2001**, *123*, 12048−12058.
(42) Zandomeneghi, G.; Krebs, M. R.; McCammon, M. G.; Fändrich, M. FTIR Reveals Structural Differences between Native Beta-Sheet Proteins and Amyloid Fibrils. *Protein Sci.* **2004**, *13*, 3314−3321.
(43) Decatur, S. M. Elucidation of Residue-Level Structure and Dynamics of Polypeptides via Isotopp-Edited Infrared Spectroscopy. *Acc. Chem. Res.* **2006**, *39*, 169−175.
(44) Ling, Y. L.; Strasfeld, D. B.; Shim, S. H.; Raleigh, D. P.; Zanni, M. T. Two-Dimensional Infrared Spectroscopy Provides Evidence of an Intermediate in the Membrane-Catalyzed Assembly of Diabetic Amyloid. *J. Phys. Chem. B* **2009**, *113*, 2498−2505.

(45) Guo, Y.; Wang, J. Spectroscopic Evidence for Polymorphic Aggregates Formed by Amyloid-Beta Fragments. *ChemPhysChem* **2012**, *13*, 3901−3908.
(46) Chirgadze, Y. N.; Nevskaya, N. A. Infrared-Spectra and Resonance Interaction of Amide-I Vibration of Anti-Parallel-Chain Pleated Sheet. *Biopolymers* **1976**, *15*, 607−625.
(47) Peralvarez-Marin, A.; Mateos, L.; Zhang, C.; Singh, S.; Cedazo-Minguez, A.; Visa, N.; Morozova-Roche, L.; Graslund, A.; Barth, A. Influence of Residue 22 on the Folding, Aggregation Profile, and Toxicity of the Alzheimer's Amyloid Beta Peptide. *Biophys. J.* **2009**, *97*, 277−285.
(48) Sarroukh, R.; Cerf, E.; Derclaye, S.; Dufrene, Y. F.; Goormaghtigh, E.; Ruysschaert, J.-M.; Raussens, V. Transformation of Amyloid Beta(1−40) Oligomers into Fibrils is Characterized by a Major Change in Secondary Structure. *Cell. Mol. Life Sci.* **2010**, *68*, 1429−1438.
(49) Celej, M. S.; Sarroukh, R.; Goormaghtigh, E.; Fidelio, G. D.; Ruysschaert, J.-M.; Raussens, V. Toxic Prefibrillar Alpha-Synuclein Amyloid Oligomers Adopt a Distinctive Antiparallel Beta-Sheet Structure. *Biochem. J.* **2012**, *443*, 719−726.
(50) Yamaoki, Y.; Imamura, H.; Fulara, A.; Wójcik, S.; Bożycki, L.; Kato, M.; Keiderling, T. A.; Dzwolak, W. An FT-IR Study on Packing Defects in Mixed Beta-Aggregates of Poly(L-Glutamic Acid) and Poly(D-Glutamic Acid): A High-Pressure Rescue from a Kinetic Trap. *J. Phys. Chem. B* **2012**, *116*, 5172−5178.
(51) Demirdöven, N.; Cheatum, C. M.; Chung, H. S.; Khalil, M.; Knoester, J.; Tokmakoff, A. Two-Dimensional Infrared Spectroscopy of Antiparallel Beta-Sheet Secondary Structure. *J. Am. Chem. Soc.* **2004**, *126*, 7981−7990.
(52) Greenfield, N. J. Using Circular Dichroism Spectra to Estimate Protein Secondary Structure. *Nat. Protoc.* **2006**, *1*, 2876−2890.
(53) Heinig, M.; Frishman, D. Stride: A Web Server for Secondary Structure Assignment from Known Atomic Coordinates of Proteins. *Nucleic Acids Res.* **2004**, *32*, W500−W502.
(54) Stine, W. B. J.; Dahlgren, K. N.; Krafft, G. A.; LaDu, M. J. In Vitro Characterization of Conditions for Amyloid-Beta Peptide Oligomerization and Fibrillogenesis. *J. Biol. Chem.* **2003**, *278*, 11612−11622.
(55) Cerf, E.; Sarroukh, R.; Tamamizu-Kato, S.; Breydo, L.; Derclaye, S.; Dufrêne, Y. F.; Narayanaswami, V.; Goormaghtigh, E.; Ruysschaert, J. M.; Raussens, V. Antiparallel Beta-Sheet: A Signature Structure of the Oligomeric Amyloid Beta-Peptide. *Biochem. J.* **2009**, *421*, 415−423.
(56) Ma, G.; Li, Y.; Dong, J.; Zou, Y.; Zhang, Z.; Sun, Y. The Dynamic Nature of Incubation Solution after Cooling to Room Temperature in Amyloid Formation of Hen Egg White Lysozyme: An FTIR Assessment. *Vib. Spectrosc.* **2013**, *64*, 44−50.
(57) Lührs, T.; Ritter, C.; Adrian, M.; Riek-Loher, D.; Bohrmann, B.; Döbeli, H.; Schubert, D.; Riek, R. 3D Structure of Alzheimer's Amyloid-Beta(1−42) Fibrils. *Proc. Natl. Acad. Sci. U.S.A.* **2005**, *102*, 17342−17347.
(58) Tycko, R. Molecular Structure of Amyloid Fibrils: Insights from Solid-State NMR. *Q. Rev. Biophys.* **2006**, *39*, 1−55.
(59) Luca, S.; Yau, W. M.; Leapman, R.; Tycko, R. Peptide Conformation and Supramolecular Organization in Amylin Fibrils: Constraints from Solid-State NMR. *Biochemistry* **2007**, *46*, 13505−13522.
(60) Krimm, S.; Bandekar, J. Vibrational Analysis of Peptides, Polypeptides, and Proteins. V. Normal Vibrations of Beta-Turns. *Biopolymers* **1980**, *19*, 1−29.
(61) Strasfeld, D. B.; Ling, Y. L.; Gupta, R.; Raleigh, D. P.; Zanni, M. T. Strategies for Extracting Structural Information from 2D IR Spectroscopy of Amyloid: Application to Islet Amyloid Polypeptide. *J. Phys. Chem. B* **2009**, *113*, 15679−15691.
(62) DuBay, K. F.; Pawar, A. P.; Chiti, F.; Zurdo, J.; Dobson, C. M.; Vendruscolo, M. Prediction of the Absolute Aggregation Rates of Amyloidogenic Polypeptide Chains. *J. Mol. Biol.* **2004**, *341*, 1317−1326.
(63) Qiang, W.; Yau, W.-M.; Luo, Y.; Mattson, M. P.; Tycko, R. Antiparallel Beta-Sheet Architecture in Iowa-Mutant Beta-Amyloid Fibrils. *Proc. Natl. Acad. Sci. U.S.A.* **2012**, *109*, 4443−4448.